Received: 18 October 2021 | Revised: 12 January 2022 | Accepted: 12 February 2022

DOI: 10.1111/jace.18426

Journal of the American Ceramic Society

RESEARCH ARTICLE

The influence of the processing parameters on the reactive flash sintering of ZrO_2-CeO_2

Rubens Roberto Ingraci Neto | **Erofili Kardoulaki** | **James Anthony Valdez**

Materials Science and Technology Division, Los Alamos National Laboratory, Los Alamos, New Mexico, USA

Correspondence
Rubens Roberto Ingraci Neto, Materials Science and Technology Division, Los Alamos National Laboratory, P.O. Box 1663, Los Alamos, NM 87545, USA.
Email: rubens.ingraci@lanl.gov

Abstract

Reactive flash sintering (RFS) is a method that was recently developed to produce dense single-phase bulk ceramic parts through solid-state reactions in a single-step that only takes a few minutes. The influence of the RFS parameters on the phase purity of a simple mixed oxide, $(Zr_{0.8},Ce_{0.2})O_2$, was investigated. Parameters such as furnace temperature, furnace atmosphere, electric current density, and alternating current (AC) or direct current (DC) were examined. It was found that $(Zr_{0.8},Ce_{0.2})O_2$ pellets with high densities, above 90% of its theoretical density, can be produced by RFS in a few minutes when RFS occurs under oxidizing atmospheres, AC fields with current densities of 100 $mA{\cdot}mm^{-2}$, and at a furnace temperature of 1200°C. Reducing conditions such as Ar-H_2 atmosphere and DC fields, low furnace temperatures, and low current densities resulted in phase impurities and poor reactions between the ZrO_2 and the CeO_2 powders. These results show that RFS is a useful method to produce mixed oxides, but it is very sensitive to the processing parameters. This is the first time that the influence of most of the RFS processing parameters has been studied systematically. Thus, the present work aims to provide guidelines on selecting the right processing parameters when exploring RFS.

KEYWORDS
flash sintering, mixed oxides, reactive flash sintering, solid-state reactions, ZrO_2-CeO_2

1 | INTRODUCTION

Flash sintering (FS) was first described more than a decade ago[1] as a method that integrated high electric fields (> 50 V·cm) and electric currents (> 10 $mA{\cdot}mm^{-2}$) to the sintering process providing for unparalleled sintering rates. Yttria-stabilized zirconia was sintered to full density in less than 5 seconds at only 850°C.[1] Thereafter, most of the work focused on understanding which ceramic materials could be sintered by FS,[2,3] the fundamental science behind it,[4–15] and what were the influences of the FS parameters on the resulting materials.[16–19] FS has since ramified in multiple applications that include contactless FS,[20–22] additive manufacturing,[23–26] and a single-step synthesis and sintering method for ceramic materials.[27]

It was demonstrated recently that FS can induce solid-state reactions to produce a single-phase, dense, and

Abbreviations: AC, alternating current; DC, direct current; EDS, energy-dispersive spectroscopy; FS, flash sintering; HV, high vacuum; RFS, reactive flash sintering; SEM, scanning electron microscopy; TD, theoretical density; XRD, x-ray diffraction.

nanostructured polycrystalline mixed oxide in 1 minute from a mix of its elemental oxides.[27] This method was named reaction flash sintering or reactive flash sintering (RFS)[27–29] and it has been used to produce $BiFeO_3$,[27] $MgAl_2O_4$,[30] PbO-ZrO_2-TiO_2,[31] $Gd_2Zr_2O_7$,[32] $BaTiO_3$,[33] $Li_{5.95}Al_{0.35}La_3Zr_2O_{12}$,[34] $(Bi_{0.2}Na_{0.2}K_{0.2}Ba_{0.2}Ca_{0.2})TiO_3$,[35] $Mg_{0.2}Ni_{0.2}Co_{0.2}Cu_{0.2}Zn_{0.2}O$,[36] and $(La_{0.2}Nd_{0.2}Sm_{0.2}Eu_{0.2}Gd_{0.2})_2Zr_2O_7$[37] from a mix of their oxide powder precursors. Alternatively, RFS also works with powder precursors prepared by chemical synthesis methods.[29,38] For instance, $CaCu_3Ti_4O_{12}$ amorphous precursor powder prepared by a Pechini-derived method was sintered in a few minutes into single-phase samples with densities higher than 90% of their theoretical density (TD) by RFS in air, at furnace temperatures $\leq$ 955°C under electric field intensities $\geq$ 30 V·cm^{-1} and current densities up to 75 mA·mm^{-2}.[38,39] Additionally, other materials such as $Li_{0.5}La_{0.5}TiO_3$,[29] $Li_{6.25}Al_{0.25}La_3Zr_2O_{12}$,[40] $Mg_{0.2}Ni_{0.2}Co_{0.2}Cu_{0.2}Zn_{0.2}O$,[41] $MgTiO_3$,[42] (Zn,Cu,Co,Ni,Mg)O,[43] and $Na_3Zr_2(SiO_4)_2(PO_4)$[44] were also synthesized and sintered by RFS in air from their chemically prepared precursors. Therefore, RFS seems to be a method that can be used to synthesize and densify complex oxides in a single step in just a few minutes. Bulk samples of single-phase materials with high densities and sub-micrometric grain were obtained using RFS, as seen in FS.[30–32,42,43] The technique is even more promising when these oxides contain low meting point or volatile elements that make conventional solid-state reactions difficult or impossible. Nevertheless, RFS science is still evolving and studies about the effect of the processing parameters on the materials produced by RFS are still limited. Most RFS experiments to date have been executed in air using direct current (DC) electric fields. A summary of the processing parameters evaluated so far in the literature is presented in Table 1. Note that only two studies used alternating current (AC) for RFS, and only one happened at a different furnace atmosphere rather than air. In general, it was observed that AC electric fields can minimize electrochemical reactions induced by DC.[44] AC electric fields can also be used to produce pyrochlore phases, such as $(La_{0.2}Nd_{0.2}Sm_{0.2}Eu_{0.2}Gd_{0.2})_2Zr_2O_7$, from a mixed oxide powder precursor in oxygen-deficient atmosphere.[37] On the other hand, DC fields can induce defect formations such as oxygen deficiency in some oxide materials.[33] Finally, from the current understanding on RFS, it can also be concluded that high current densities usually enhance the phase reactions and sintering rates[34,38,39,41,43] but, if the current density increases above a certain threshold, it can cause damages to the material.[40]

A more comprehensive study of the RFS parameters and their influence on the reactions during RFS can improve the control of RFS and provide guidelines for future research. Therefore, in the present work, different effects of the RFS parameters, such as furnace temperature, furnace atmosphere, electric current density, and DC or AC modes were examined on RFS of the ZrO_2-CeO_2 system. This mixed oxide system, ZrO_2-CeO_2, was selected as a surrogate for many oxide solid solution systems. Additionally, there are only two cations in this system, which should facilitate the interpretation of the RFS results. The ZrO_2-CeO_2 system is also of interest because it is used in fuel cells, gas sensors, solid-state electrolytes, biomaterials, and widely employed in the automotive industry for pollution control as a three-way catalyst due to its ability to produce CO and H_2 from CO_2 and H_2O.[45,46]

2 | METHODS

A mixture of 80 mol% of monoclinic ZrO_2 (TZ-0 from Tosoh) with 20 mol% of CeO_2 (REacton) was prepared by high-energy ball milling (SPEX Certiprep) of the dry powders without any additive or binder for 1 hour in an alumina jar with ZrO_2 ball. The mixed powder was then granulated through a 200-mesh sieve (74 μm), and cold pressed at 200 MPa into pellets that were 5.33 mm in diameter and 4.0 ±0.2 mm long with a green density of 61 ± 1% TD.

RFS tests were performed in a dilatometer (DIL 402C from Netzsch) that was adapted by inserting two platinum electrodes into its furnace chamber, as described elsewhere.[47,48] Two power supplies were used in this study, one for DC fields (N5772A from Keysight) and another for AC fields set at 16 Hz (AST1501 from California Instruments). The bottom and top surfaces of the 0.8(ZrO_2)+0.2(CeO_2) pellets were painted with platinum paint to improve the electrical contact between pellet and electrodes. Once a pellet was loaded into the dilatometer, and the furnace chamber was closed, the chosen atmosphere was created. Three different atmospheres were tested, high vacuum (HV) at < 7·10^{-3} Pa, air flowing at 200 mL·min^{-1}, or Ar-6 vol%H_2 also flowing at 200 mL·min^{-1}. The RFS tests were performed using the controlled current-rate approach. This approach contributes to the grain size homogeneity between electrodes and minimizes the current localization and thermal shock.[19,48] After the sample was preheated, the maximum electric field was applied and the current permitted through the sample was increased linearly at a predefined rate. The current rates were defined in such a way that it always took 1 minute to reach the preset maximum current densities. After 2 minutes at the maximum current, the electric current was shut off and the furnace cooled down.

To understand the influence of different processing parameters on the RFS of the 0.8(ZrO_2)+0.2(CeO_2) mix, an experimental plan was designed and it is outlined in Table 2. First, the influence of the atmosphere in RFS

TABLE 1 Summary of the reactive flash sintering (RFS) parameters investigated in the literature

Material	Precursor	Furnace atm.	Furnace temp. (°C)	Voltage mode	E ($V \cdot cm^{-1}$)	J ($mA \cdot mm^{-2}$)	Results	Ref.
$BiFeO_3$	Mixed oxides powders	Air	570-625	DC	25-100	20-50	Single phase in 60 s, 87% TD	27
$MgAl_2O_4$		Air	730-950	DC	300-1000	60	Single phase ~60 s, > 93% TD Average grain sizes from 0.37 to 0.47 μm 8YSZ added to induce RFS	30
$PbO\text{-}ZrO_2\text{-}TiO_2$		Air	520-570	DC	300-600	37	Single phase in 30 s, > 96% TD Average grain sizes increase with the electric field from 0.3 to 0.95 μm	31
$Gd_2Zr_2O_7$		Air	1050	DC	100	83	Single phase in 60 s Defect fluorite phase annealed to pyrochlore Average grain sizes 0.36-0.49 μm	32
$BaTiO_3$		Air	960-1007	DC	100-300	23.5	Tetragonal and hexagonal phases in 30 s Oxygen deficiency triggered cubic to hexagonal phase transition	33
$Li_{5.95}Al_{0.35}La_3Zr_2O_{12}$		Air	~ 700	DC	20-50	160-200	Predominantly single phase in ~60 s, 86% TD	34
$(Bi_{0.2}Na_{0.2}K_{0.2}Ba_{0.2}Ca_{0.2})TiO_3$		Air	840	DC	200	20-30	Single phase in 280 s, fully dense	35
$Mg_{0.2}Ni_{0.2}Co_{0.2}Cu_{0.2}Zn_{0.2}O$		Air	~ 25	DC	250	80	Single phase in 60 s, 62% TD	36
$(La_{0.2}Nd_{0.2}Sm_{0.2}Eu_{0.2}Gd_{0.2})_2Zr_2O_7$		Vacuum (5 Pa)	1200	AC (100 Hz)	90	60-200	Single phase in ~60 s, 99% TD	37
$CaCu_3Ti_4O_{12}$	Chemically prepared	Air	750-1050	DC	10-200	5-75	Single phase in ~60 s, > 90% TD	38,39
$Li_{0.5}La_{0.5}TiO_3$		Air	800-950	DC	80-120	60	Single phase in 45 s, > 96% TD	29
$Li_{6.25}Al_{0.25}La_3Zr_2O_{12}$		Air	600	DC	50	150	Single phase in 30 s, > 90% TD Secondary phase if > 150 mA mm-2	40
$Mg_{0.2}Ni_{0.2}Co_{0.2}Cu_{0.2}Zn_{0.2}O$		Air	450-1000	DC	15-60	30 to 500	Single phase in 60s, > 77% TD	41
$MgTiO_3$		Air	1128-1241	DC	500-800	37	Single phase in 30 s, up to 97.6% TD Average grain size from 0.07 to 1.2 μm	42
(Zn,Cu,Co,Ni,Mg)O		Air	350	DC	100	600-900	Single phase in 3 min, > 92% TD Average grain size from 1 to 2 μm	43
$Na_3Zr_2(SiO_4)_2(PO_4)$		Air	700	DC or AC (800 Hz)	45	60	Almost single phase in 30 s, > 90% TD using AC DC resulted in a secondary phase ($Na_2ZrSi_2O_7$) and incomplete reaction with NaO_x accumulated at the cathode	44

TABLE 2 Experimental conditions for reactive flash sintering (RFS) of $0.8(ZrO_2)+0.2(CeO_2)$ powder mixture

Group	Temperature (°C)	Atmosphere	Electric field ($V \cdot cm^{-1}$)	Current density ($mA \cdot mm^{-2}$)	Current mode
1	1200	Ar+6 vol%H_2	250	100	AC
		HV			
		Air			
2	800	Best from 1 (air)	1325	100	DC
	1000		1000		
	1200		250		
3	Best from 2 (1200°C)		250	25	Best mode (AC)
				50	
				100	
Baseline	1200	Air	–	–	–
	1200	HV			

Note: The best parameters indicated between brackets were chosen from the results achieved at the previous group based on the x-ray diffraction (XRD) data. For all tested conditions the furnace heating rate was $10°C \cdot min^{-1}$ and the pellets were let to cool down naturally at approximately $30°C \cdot min^{-1}$.
Abbreviations: AC, alternating current; DC, direct current; HV, high vacuum.

was studied using three different furnace atmospheres: air as an oxidizing atmosphere, HV as an oxygen-deficient medium, and Ar-6 vol%H_2 as a reducing gas. The pellets were preheated to 1200°C at $10°C \cdot min^{-1}$ under these different atmospheres and then subjected to an AC electric field of 250 $V \cdot cm^{-1}$ to induce RFS. The electric current flowing through the pellet was increased linearly using a controlled current rate taking 1 minute to reach its maximum value. The pellets were held for 2 minutes under the maximum electric current density, 100 $mA \cdot mm^{-2}$. After RFS, the pellets were let to cool down naturally inside the adapted dilatometer at a cooling rate of approximately $30°C \cdot min^{-1}$. From this test group, the best atmosphere was selected and the next stage was to determine the best isothermal temperature to induce RFS. Thus, in the second test group, three tests were carried out at 800°C and 1325 $V \cdot cm^{-1}$, 1000°C and 1000 $V \cdot cm^{-1}$, and 1200°C and 250 $V \cdot cm^{-1}$, where the DC electric field intensity was identified as the minimum necessary to promote the onset of RFS. The current density limit of these tests was again kept at 100 $mA \cdot mm^{-2}$ for 2 minutes and the same current rate was used, 100 $mA \cdot mm^{-2} \cdot min^{-1}$. Finally, the best temperature, electric field intensity, atmosphere, and current mode (AC or DC) combination was selected and the maximum current density was limited to 25 $mA \cdot mm^{-2}$, 50 $mA \cdot mm^{-2}$, or 100 $mA \cdot mm^{-2}$. For each current density limit, the current rate was adjusted for 1 minute to the maximum value. Additionally, two baseline tests were carried out, where no electric field was applied. The samples were only heated up at $10°C \cdot min^{-1}$ under air or HV up to 1200°C and then held for 15 minutes at that temperature to create baselines for what conventional solid-state reaction results would be at high temperatures and short reaction times.

The produced pellets were later characterized by scanning electron microscopy (SEM) using an FEI Apreo microscope equipped with an energy-dispersive spectroscopy (EDS) detector (Octane Elite EDAX) to create the elemental mapping of the cross-sections of the pellets. In addition, the densities of the produced pellets were measured by Archimedes' method. The phases of the samples were identified by x-ray diffraction (XRD) using a Bruker D8 Advance in a Bragg-Brentano geometry using a Cu Kα source (Kα1 = 1.5406 Å) set to 40 mA and 40 kV and a LYNXEYE XE-T detector. The samples were prepared for the XRD analysis by polishing their extremities to remove the platinum paste contamination and then the pellets were ground in an Al_2O_3 mortar and pestle. Hence, the XRD patterns collected reflect the average of the entire composition of the pellets. Whole pattern fitting and Rietveld refinement were performed using MDI JADE software.[49] The patterns were refined as an attempt to identify their composition as well as their phase fractions through their lattice parameters. The results of the refinement are shown in the supplementary material, in Figure S1.

The black body radiation model[8] was used to estimate the temperature of the samples during RFS. The model is defined in Equation 1, where T is the sample average absolute temperature, T_f is the furnace absolute temperature, P_W is the electric power (W), A_s is the surface area (m^2) transferring heat by radiation to the furnace, and σ is the Stefan-Boltzmann constant ($5.67 \cdot 10^{-8}$ $W \cdot m^{-2} \cdot K^{-4}$)

$$T = T_f \left(1 + \frac{P_W}{\sigma A_s T_f^4}\right)^{\frac{1}{4}} \quad (1)$$

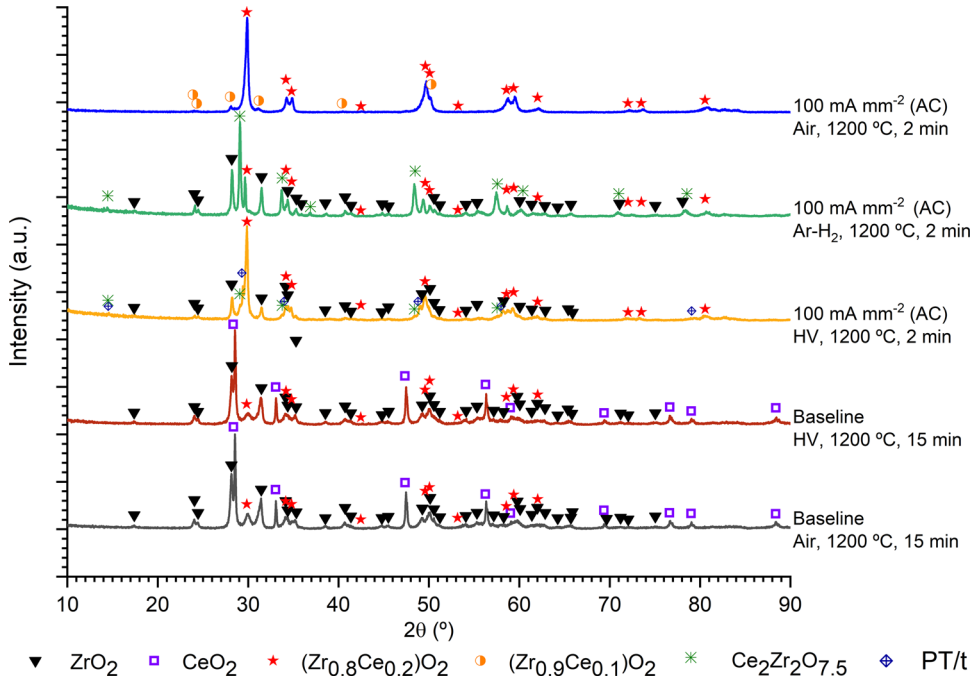

FIGURE 1 X-ray diffraction (XRD) patterns of $0.8(ZrO_2)+0.2(CeO_2)$ mixed powders after reactive flash sintering (RFS) at different atmospheres. Baseline conditions were conventional heat treatments at the specified atmosphere, temperature, and dwell time at the maximum temperature. RFS conditions are indicated by the current density limit (100 $mA{\cdot}mm^{-2}$ AC) for all tests. Atmospheres tested were air, high vacuum (HV), and Ar + 6 vol% H_2

The actual temperatures of the pellets were probably a couple hundred degrees lower than the estimates, since the aspect ratio of the pellets (4:3 – diameter vs. length) was different from the traditional dog-bone shaped samples from the literature (1:8 thickness vs. length[16]). It is also known that a fraction of the heat will be dissipated by thermal conduction through the top and bottom of the pellet in contact with the electrodes.[48] Yet, the black body radiation model offers a good approximation when the pellet temperature during RFS and the furnace temperature are not too different, since thermal radiation would still be the dominant heat transfer mechanism.

3 | RESULTS

The first step of this comprehensive study was to investigate the effect of the furnace atmosphere on the RFS reactions, as delineated at group 1 in Table 2. The XRD patterns of the samples after RFS at different furnace atmospheres are presented in Figure 1, as well as the XRD patterns for the baseline tests performed under air flow and HV. It is evident that RFS caused a reaction between the precursor powders leading to the formation of $(Zr_{0.8},Ce_{0.2})O_2$ as tetragonal phase when RFS happened in air at 1200°C. Moreover, the phase purity achieved by RFS in air was much higher than the one attained by the baseline test in air, where almost no $(Zr_{0.8},Ce_{0.2})O_2$ was formed. When performing RFS under reducing atmosphere (Ar + 6 vol% H_2) or HV, the transformation to $(Zr_{0.8},Ce_{0.2})O_2$ was incomplete and led to the formation of a pyrochlore phase, $Ce_2Zr_2O_{7.5}$, when under reducing atmosphere and probably to an oxygen-rich pyrochlore-type phase or to metastable tetragonal phases under HV, indicated in Figure 1 by *PT/t*.

The synthesis of the tetragonal phase of $(Zr_{0.8}Ce_{0.2})O_2$ was the main product from RFS in air at 1200°C and 250 $V{\cdot}cm^{-1}$ up to 100 $mA{\cdot}mm^{-2}$, but some monoclinic $(Zr_{0.9}Ce_{0.1})O_2$ phase was also identified. These phases, tetragonal and monoclinic, could be expected from the nominal composition of the mixture according to the phase equilibrium diagram of the ZrO_2-CeO_2 system.[50] Indeed, the presence of these phases at room temperature after mixtures of $0.8(ZrO_2)+0.2(CeO_2)$ were heat treated at temperatures ≥ 1350°C was reported in the literature.[51,52] Joule heating caused by the electric current during RFS was expected to increase the sample temperature further than the furnace temperature. According to the black body radiation model,[8] Equation 1, the average temperature during RFS at the maximum current density (100 $mA{\cdot}mm^{-2}$) under air was 1690°C. As explained before in the Methods section, this value is likely to be overestimated because the pellet was also losing heat by thermal conduction through its bottom and top surfaces that were in contact

with the platinum electrodes. However, according to the ZrO_2-CeO_2 system phase equilibrium diagram,[50] between 1300°C and 1700°C, a fully tetragonal phase is expected for $(Zr_{0.8}Ce_{0.2})O_2$, and the RFS temperature was likely within this temperature range. The average temperatures reached by the samples that were exposed to Ar-H_2 and HV were 1690°C and 1580°C, respectively.

The Rietveld refinement of the XRD patterns indicated that RFS under air at 1200°C and 250 V·cm^{-1} AC up to 100 mA·mm^{-2} resulted in the formation of 94 vol.% of tetragonal phase of $(Zr_{0.8}Ce_{0.2})O_2$ ($P4_2/nmc$) and 6 vol.% of monoclinic phase ($P2_1/c$). The pattern was refined with a goodness of fit (X^2) equal to 1.37 considering the tetragonal phase for $(Zr_{0.8}Ce_{0.2})O_2$ with lattice constants $a = 3.6371(1)$ Å, $c = 5.2401(1)$ Å, and the monoclinic phase $(Zr_{0.9}Ce_{0.1})O_2$ with $a = 5.1934(2)$ Å, $b = 5.2254(2)$ Å, and $c = 5.3639(2)$ Å as described by Varez et al. (2007).[53]

RFS under Ar-H_2 atmosphere resulted in 52.3 vol.% of monoclinic ZrO_2, from Rietveld refinement using the ICSD entry code 80043, 35.3 vol.% of pyrochlore $Ce_2Zr_2O_{7.5}$, and 12.4 vol.% of tetragonal phase $(Zr_{0.8}Ce_{0.2})O_2$. The refinement of the pyrochlore phase $Ce_2Zr_2O_{7.5}$ (F-43 m) was performed using the phase described by Achary et al. (2009)[54] with lattice constant $a = 10.61007(23)$ Å from the ICSD entry code 420823. The refinement of the pattern had a X^2 of 1.22.

RFS using AC mode under oxygen-deficient condition, HV, led to the formation of approximately 48.3 vol.% of the tetragonal phase $(Zr_{0.8}Ce_{0.2})O_2$, while monoclinic ZrO_2 was 22.5 % of the volume, the pyrochlore phase $Ce_2Zr_2O_{7.5}$ was only 2.4 vol.%, and the remaining 26.8 vol.% was probably an oxygen-rich pyrochlore-type phase $(Zr_2Ce_2O_{7+x})$ with $0.5 < x \geq 1$ or a metastable tetragonal phase. The Rietveld refinement indicated that the Ce/Zr ratio for this phase was close to 0.5. This can be attributed to the formation of an oxygen-rich pyrochlore-type phase that has a superlattice structure.[54–56] This cubic fluorite phase can have lattices parameter ranging from $a = 10.5443$ Å to 10.6924 Å.[54] However, these oxygen-rich pyrochlore-type phases show diffraction peaks very similar to the metastable tetragonal phases, t' and t'', which could be formed from the pyrochlore phase, which is also metastable.[56] Therefore, the weak diffraction lines around 14.5° and 36.9° were indicative that both pyrochlore and tetragonal phases could be present.

The second series of tests, group 2 in Table 2, was then carried out in air. The XRD patterns obtained after RFS at different furnace temperatures and electric fields are shown in Figure 2. Temperatures above 1000°C were necessary to induce RFS. At 800°C, RFS could not be induced even at a high electric field, 1325 V·cm^{-1}. Moreover, incomplete transformations were observed in all tested conditions using DC electric fields. Residual monoclinic ZrO_2 was present when using DC electric fields and pyrochlore-type phase or metastable tetragonal phases were obtained at 1000°C and 1200°C. On the other hand, the XRD pattern for RFS in air under AC mode at the same temperature and electric current density was free of residual ZrO_2 and had no apparent pyrochlore phase. The estimated average temperature reached at maximum current density was 1590°C for RFS in air using DC mode and furnace temperature of 1200°C and 1760°C for RFS in air using DC mode and furnace temperature of 1000°C.

The refinement of the XRD pattern (X^2 of 1.32) indicated that RFS at 1200°C using DC mode promoted the formation of 43.5 vol.% of tetragonal $(Zr_{0.8}Ce_{0.2})O_2$ and 21.6 vol.% of oxygen-rich pyrochlore-type phase or metastable tetragonal phases. In addition, residual monoclinic ZrO_2 represented 34.9 vol.%. RFS using DC mode at 1000°C could not be refined with reasonable precision.

The results reported so far indicated that better phase purity could be obtained when carrying out RFS under oxidizing atmospheres using AC electric field at 1200°C. Yet, another reason for choosing 1200°C as the best condition was the stability of the electric power flowing through the material during the RFS, as seen in Figure 3 for DC electric fields. Since RFS at 1200°C happened at lower electric field, 250 Vcm^{-1} versus 1000 V·cm^{-1} at 1000°C, the fluctuations in the DC electric field and therefore in the power density were smaller. Lower electric fields are also less predisposed to cause thermal shock during RFS onset. Moreover, at the highest furnace temperature the electrical conductivity of the oxide material was higher, 0.32 S·m^{-1} at 1200°C against 0.19 S·m^{-1} at 1000°C, helping to stabilize the process. The electric field stability, as exhibited in Figure 3, is important because it provides better control of the RFS process, eliminating variability in the results.

An analogous instability in the electric field and power density was also observed when contrasting RFS under air and reducing atmospheres using AC mode and furnace temperature of 1200°C. After reaching the maximum current density of 100 mA·mm^{-2} the fluctuations in the electric field, electric current, and thus in the power density were intenser in the reducing atmosphere condition, as indicated in Figure 4. Additionaly, the difference in the electric current profile between DC and AC is noticeable. While the electric current was well regulated under DC mode, as seen in Figure 3, the electric current oscillated in the AC mode while ramping up. However, these behaviors were intrinsic to the two power supply units used. The characteristics of each power supply unit must be taken in account to ensure the smoothest power flow as possible to avoid damage by thermal shocks, hot spots, and current localization.

Finally, the electric current density effect on the phase transformation was analyzed through RFS tests in air

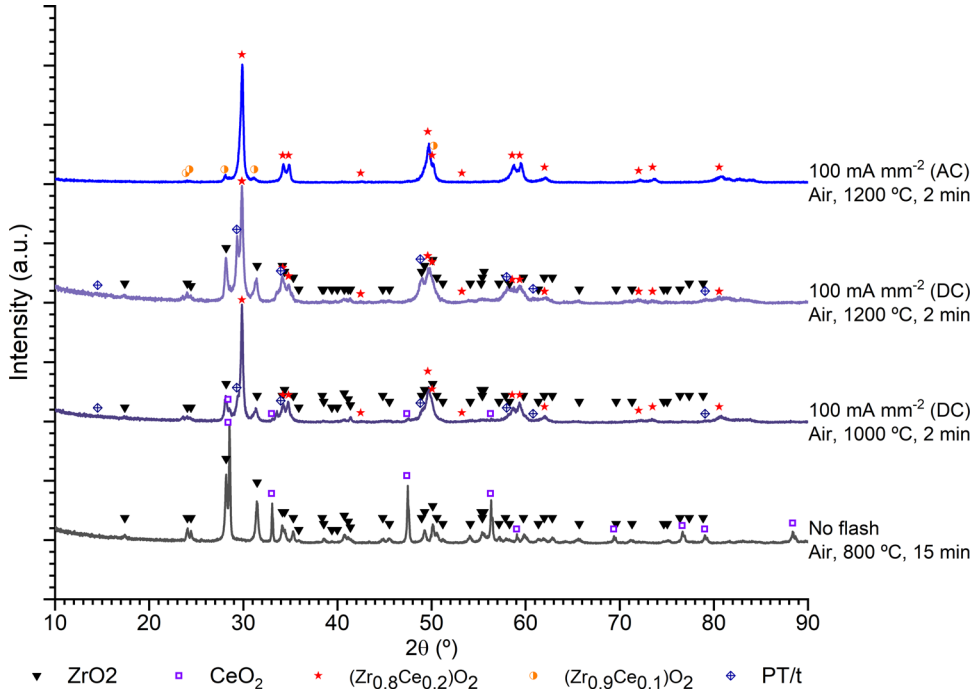

FIGURE 2 X-ray diffraction (XRD) patterns showing the effect of the temperature and current mode (direct current [DC] vs. alternating current [AC]) on the reactive flash sintering (RFS) of $0.8(ZrO_2)+0.2(CeO_2)$ into $(Zr_{0.8}Ce_{0.2})O_2$

at 1200°C under 250 V·cm^{-1}. As presented in the XRD patterns in Figure 5, higher current densities improved the RFS reactions, while residual CeO_2 and ZrO_2 peaks were still present in the XRD patterns of the samples after RFS at low current densities, 25 mA·mm^{-2} and 50 mA·mm^{-2}. The estimated average temperatures were 1690°C, 1580°C, and 1470°C for RFS at 100 mA·mm^{-2}, 50 mA·mm^{-2}, and 25 mA·mm^{-2}, respectively. Therefore, it is possible that the incomplete phase transformations could be related to the lower temperatures achieved at different current densities. The Rietveld refinement of the patterns indicated the presence of residual monoclinic ZrO_2 at 7.6 vol.% and cubic fluorite CeO_2 (ICSD entry code 185143) at 5.0 vol.% after RFS up to 50 mA·mm^{-2}. Likewise, tetragonal $(Zr_{0.8}Ce_{0.2})O_2$ represented 81.5 vol.% and monoclinic $(Zr_{0.9}Ce_{0.1})O_2$ accounted for 5.9 vol.%, in contrast to 94 vol.% of the tetragonal phase attained after RFS up to 100 mA·mm^{-2}. Residual CeO_2 was also observed at 25 mA·mm^{-2} in a concentration of 5.7 vol.%, as well as ZrO_2 at 11.6 vol.% The tetragonal and the monoclinic phases represented 72.7 vol.% and 10 vol.%, respectively. A X^2 below 1.3 was obtained for all the refinements.

It can be concluded that the mixed oxide $Zr_{0.8}Ce_{0.2}O_2$ could be produced by RFS of the $0.8(ZrO_2)+0.2(CeO_2)$ powder mixture, and that the use of an oxidizing atmosphere, AC electric field, and high current densities were essential to guarantee better phase purity as seen in the XRD patterns. The microstructure of the samples produced by RFS under air and under Ar-H_2 at 1200°C up to 100 mA mm^{-2} are presented in Figure 6. The elemental mapping revealed that the microstructures were homogeneous, with a few regions being richer in CeO_2 or ZrO_2, probably because of incomplete mixing of the precursor powders. Further mixing is an alternative to improve the homogeneity of the microstructure. The contamination by Al_2O_3 was less than 1.5 wt.% is probably due to the ball milling step in an Al_2O_3 jar, and was not identified by the XRD analysis. On the other hand, the pellet produced under the oxidizing condition was dense, 5.93 g cm^{-3}, with low porosity. According to the lattice parameters extracted from the XRD pattern for tetragonal $(Zr_{0.8}Ce_{0.2})O_2$, $a = 3.64$ Å, $c = 5.24$ Å, its full density was estimated as 6.30 g·cm^{-3}, hence, the pellet obtained by RFS was about 94 %TD.

Still regarding the homogeneity of the pellets after RFS, it is important to indicate that the microstructures of the pellets were not affected by current localization or hot spots, even though high electric fields and oxygen-deficient or reducing atmospheres were investigated. These results are probably due to the adoption of the controlled current-rate approach and because of the pellet and electrode geometries. It is demonstrated in the literature that the current-rate approach can minimize current localization and heterogeneities in the microstructure.[19] Likewise, the green pellets in this study had a 3:4 aspect ratio (length to diameter), which means that the surface areas in contact with the platinum flat disc electrodes were high. Thus, the electric current might have been

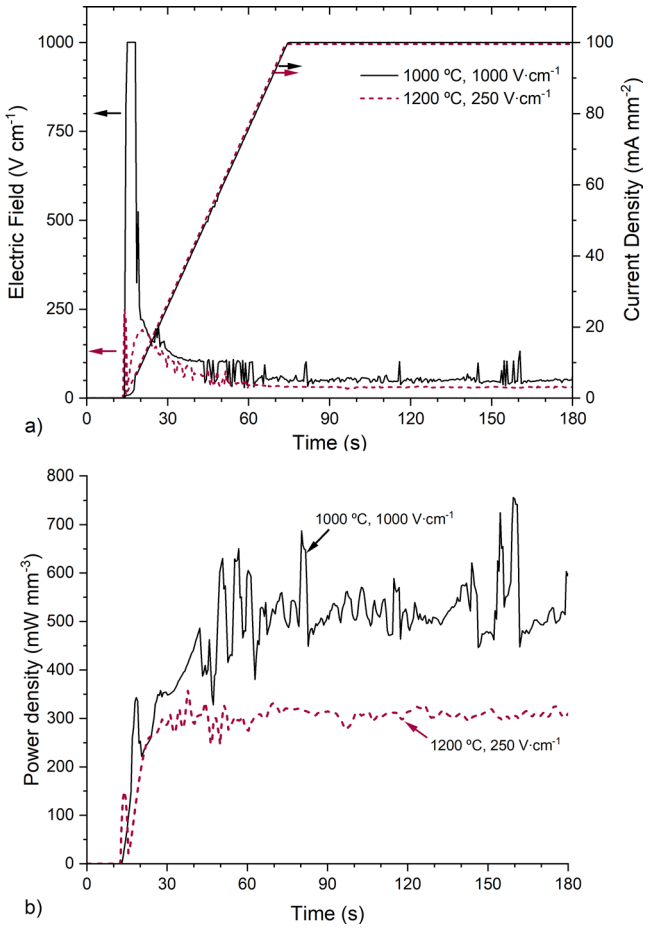

FIGURE 3 Electric field and power density evolution during reactive flash sintering (RFS) in air at different processing parameters using direct current (DC) mode. RFS onset at 1000°C under 1000 V·cm^{-1} versus RFS onset at 1200°C under 250 V·cm^{-1}

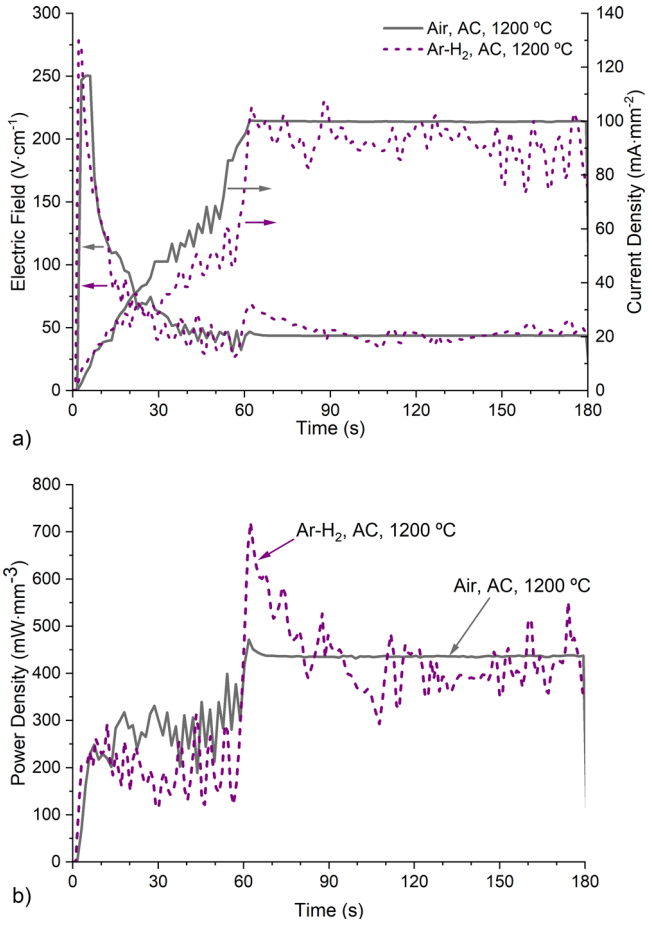

FIGURE 4 Electric field and power density evolution during reactive flash sintering (RFS) under oxidizing and reducing atmospheres using alternating current (AC) mode. (A) Electric field and electric current profiles. (B) Power density profiles

distributed homogeneously across the microstructure. Usually, dog-bone shaped samples such the ones used in the literature are more susceptible to the formation of hot spots and to current localization due to the poor contact between the platinum wire electrodes and the samples.

4 | DISCUSSION

Using the right processing parameters, RFS enhanced the solid-state reaction promoting full transformation of the powder mixture into $(Zr_{0.8}Ce_{0.2})O_2$ with a small fraction reacting to form $(Zr_{0.9}Ce_{0.1})O_2$. RFS was not only capable of synthesizing the mixed oxide in a few minutes, but it also sintered the pellets to densities up to 94 %TD, similarly to the results reported in the literature.[30,31,37]

The influence of each RFS processing parameter could be assessed individually from the results. First, it was seen that an oxidizing atmosphere (air) could promote the desired reactions to obtain the mixed oxide, $(Zr_{0.8}Ce_{0.2})O_2$, phase, while the reactions were hindered under an oxygen-deficient medium (HV). Moreover, a reducing gas (Ar-6 vol%H_2) induced the formation of a pyrochlore phase, $Ce_2Zr_2O_{7.5}$. The present work seems to be the first time RFS was performed under a reducing atmosphere, the only pyrochlore produced by RFS before, $(La_{0.2}Nd_{0.2}Sm_{0.2}Eu_{0.2}Gd_{0.2})_2Zr_2O_7$,[37] was reacted under vacuum. In general, oxygen-deficient or reducing atmospheres would increase the oxygen defect generation during RFS and produce different phases.

The electric current mode, DC or AC, showed an effect similar to the furnace atmosphere. DC mode not only impeded full reaction of the mixture but also seems to have generated a pyrochlore-type phase even in air, which was not observed under the same RFS conditions when AC mode was used in air. The electrochemical reactions that happened when using DC mode were also observed in $Na_3Zr_2(SiO_4)_2(PO_4)$[44] with the formation of a secondary phase, $Na_2ZrSi_2O_7$, and accumulation of NaO_x at the cathode. DC reducing effects were also observed in

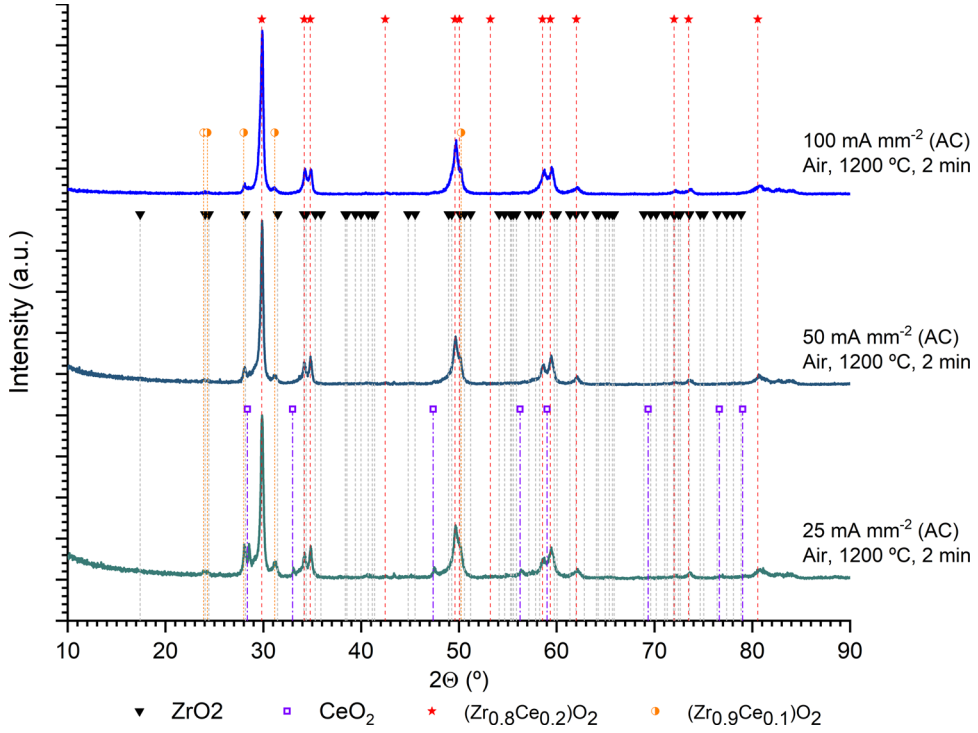

FIGURE 5 X-ray diffraction (XRD) patterns showing incomplete solutionization of the mixture $0.8(ZrO_2)+0.2(CeO_2)$ after reactive flash sintering (RFS) at different current densities. The furnace was kept at 1200°C under an air flow and the electric current was held at its maximum intensity for 2 minutes

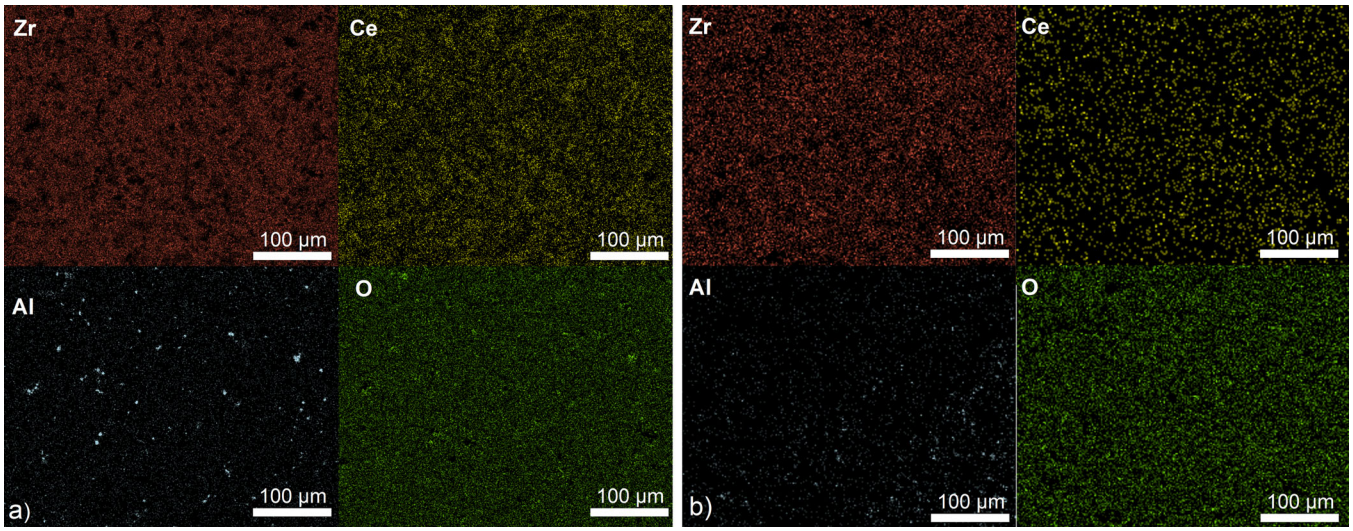

FIGURE 6 Microstructures of the $0.8(ZrO_2)+0.2(CeO_2)$ pellets after reactive flash sintering (RFS) at 1200°C up to 100 mA·mm^{-2}. (A) RFS under air. (B) RFS under Ar-H_2

air in the literature when creating defect fluorite phases of $Gd_2Zr_2O_7$,[32] and also by triggering cubic to hexagonal phase transitions in $BaTiO_3$.[33]

Intensity of the reactions was dictated by the maximum current density achieved during RFS. Tests under the same condition (onset at 1200°C und 250 V·cm^{-1}, AC mode, in air) at different current densities indicated that a certain current density intensity is necessary to promote full reaction. This is in good agreement to what was reported in the literature.[34,38,39,41,43] In general, it was observed that higher current densities led to higher temperatures during RFS, which is expected to play a major role in the reactions.

Nevertheless, the RFS onset temperature and its reciprocal electric field intensity were deemed as parameters that should be tuned to a specific material system to guarantee not only that full reactions can occur, but also that RFS

can be reliably controlled. Onset temperature influences the materials properties, such as its electrical and thermal conductivities, in such way that it can influence the quality of the microstructure produced. For instance, fluctuations in the power density could cause thermal shock and generate cracks; or high electric fields could induce current localization through the sample leading to inhomogeneous microstructure.

A guideline for choosing adequate RFS processing parameters can then be conceived:

- RFS atmosphere – The phases obtained from RFS are strongly dependent on the atmosphere composition. Oxidizing atmospheres can probably enhance the solid-state reactions promoting full phase transformation in certain oxides systems, resulting in the expected phases from the phase equilibrium diagram. Oxygen-deficient or reducing atmospheres, on the other hand, could be utilized when the creation of oxygen defects is of interest, or when trying to obtain a pyrochlore phase from a mixture of its elemental oxides.
- Electric current mode – AC mode can minimize electrochemical reduction, therefore it can promote reactions that are more homogeneous and generate phase pure materials. DC mode would favor electrochemical reduction and creation of defects, which could be useful when trying to obtain certain phases, such as a pyrochlore or metastable phases.
- RFS onset temperature and electric field – Usually temperatures higher than the minimum necessary to induce RFS should be used. Very low onset temperatures would require high electric fields, which can be problematic, as they favor power peaks, hot spots, thermal shocks, and current localization. It is also important to consider that if the power supply unit is operating near its voltage limit, its behavior can be less reliable.
- Maximum current density – High current densities would favor complete reactions and full sintering. However, extremely high current densities would likely cause damages to the material such as hot spots, grain coarsening, current localization, thermal shock, and in some cases it could cause different phases to form. It is noteworthy that the appropriate intensity of the electric current density during RFS depends on the electrical conductivity of the material and the phases that are being generated, as well as the sample geometry and electrode-sample contact resistance.

5 | CONCLUSION

A comprehensive assessment of the influence of the RFS parameters on the synthesis and sintering of $(Zr_{0.8},Ce_{0.2})O_2$ mixed oxide was performed. The importance of the processing parameters such as furnace temperature and electric field intensity, atmosphere composition, electric current mode, and current density was elucidated. It was demonstrated that RFS is a viable method to produce $(Zr,Ce)O_2$ mixed oxides resulting in fast phase transformations and high density pellets. Under the right conditions, namely, oxidizing atmospheres under AC mode with high current densities and at a certain furnace temperature, full reactions and homogeneous microstructures were obtained. Additionally, it was shown that reducing conditions, such as Ar-H_2 atmosphere and DC mode, low furnace temperatures, and low current densities could result in formation of different phases and poor reactions. Finally, a few guidelines were devised to help future work on RFS.

ACKNOWLEDGMENTS

This work was performed at Los Alamos National Laboratory, which is operated by Triad National Security, LLC, for the National Nuclear Security Administration of the U.S. Department of Energy under contract number 89233218CNA000001.

AUTHOR CONTRIBUTIONS

Rubens Roberto Ingraci Neto: Research design, investigation, data analysis, writing - original draft, writing - review and editing, Leader; Erofili Kardoulaki: Investigation, funding acquisition, writing - original draft, writing - review and editing, Advisor; Jmaes Anthony Valdez: Data acquisition, data analysis, writing - original draft, writing review and editing. Collaborator.

ORCID

Rubens Roberto Ingraci Neto https://orcid.org/0000-0003-3064-9460

REFERENCES

1. Cologna M, Rashkova B, Raj R. Flash sintering of nanograin zirconia in <5 s at 850°C. J Am Ceram Soc. 2010;93(11):3556–59.
2. Dancer CEJ. Flash sintering of ceramic materials. Mater Res Express. 2016;3(10):102001.
3. Yu M, Grasso S, McKinnon R, Saunders T, Reece MJ. Review of flash sintering: materials, mechanisms and modelling. Adv Appl Ceram. 2016;116(1):24–60.
4. M'Peko JC, Francis JSC, Raj R, Lupascu D. Impedance spectroscopy and dielectric properties of flash versus conventionally sintered yttria-doped zirconia electroceramics viewed at the microstructural level. J Am Ceram Soc. 2013;96(12):3760–7.
5. Lebrun JM, Morrissey TG, Francis JSC, Seymour KC, Kriven WM, Raj R, et al. Emergence and extinction of a new phase during on–off experiments related to flash sintering of 3YSZ. J Am Ceram Soc. 2015;98(5):1493–7.

6. Biesuz M, Sglavo VM. Microstructural temperature gradient-driven diffusion: Possible densification mechanism for flash sintering of zirconia?. Ceram Int. 2019;45(1):1227–36.
7. Yoon B, Yadav D, Raj R, Sortino E, Ghose S, Sarin P, et al. Measurement of O and Ti atom displacements in TiO_2 during flash sintering experiments. J Am Ceram Soc. 2017;101(5):1811–7.
8. Raj R. Joule heating during flash-sintering. J Eur Ceram Soc. 2012;32(10):2293–301.
9. Lebrun JM, Hellberg CS, Jha SK, Kriven WM, Steveson A, Seymour KC, et al. In-situ measurements of lattice expansion related to defect generation during flash sintering. J Am Ceram Soc. 2017;100(11):4965–70.
10. Jha SK, Terauds K, Lebrun J-M, Raj R. Beyond flash sintering in 3 mol % yttria stabilized zirconia. J Ceram Soc Jpn 2016;124(4):283–8.
11. Raj R, Chan H. Analysis of the power density at the onset of flash sintering. J Am Ceram Soc. 2016;99(10):3226–32.
12. Mishra TP, Avila V, Neto RRI, Bram M, Guillon O, Raj R. On the role of Debye temperature in the onset of flash in three oxides. Scripta Mater. 2019;170:81–4.
13. Jongmanns M, Raj R, Wolf DE. Generation of Frenkel defects above the Debye temperature by proliferation of phonons near the Brillouin zone edge. New J Phys. 2018;20(9):093013.
14. Yadav D, Raj R. Two unique measurements related to flash experiments with yttria-stabilized zirconia. J Am Ceram Soc. 2017;100(12):5374–8.
15. Yoon B, Yadav D, Ghose S, Sarin P, Raj R. On the synchronicity of flash sintering and phase transformation. J Am Ceram Soc. 2019;102(6):3110–6.
16. Francis JSC, Raj R, Halloran J. Influence of the field and the current limit on flash sintering at isothermal furnace temperatures. J Am Ceram Soc. 2013;96(9):2754–8.
17. Kumar MK P, Yadav D, Lebrun J-M, Raj R. Flash sintering with current rate: a different approach. J Am Ceram Soc. 2018;102(2):823-35.
18. Mishra TP, Neto RRI, Speranza G, Quaranta A, Sglavo VM, Raj R, et al. Electronic conductivity in gadolinium doped ceria under direct current as a trigger for flash sintering. Scripta Mater. 2020;179:55–60.
19. Mishra TP, Neto RRI, Raj R, Guillon O, Bram M. Current-rate flash sintering of gadolinium doped ceria: microstructure and defect generation. Acta Mater. 2020;189:145–53.
20. Sortino E, Lebrun JM, Sansone A, Raj R. Continuous flash sintering. J Am Ceram Soc. 2017;101(4):1432–40.
21. Saunders T, Grasso S, Reece MJ. Ultrafast-contactless flash sintering using plasma electrodes. Sci Rep. 2016;6:27222.
22. Johnson SL, Venugopal G, Hunt AT. Flame-assisted flash sintering: a noncontact method to flash sinter coatings on conductive substrates. J Am Ceram Soc. 2017;101(2):536–41.
23. Dong J, Wang Z, Zhao X, Biesuz M, Saunders T, Zhang Z, et al. Contactless flash sintering based on cold plasma. Scripta Mater. 2020;175:20–3.
24. Hagen D, Beaman JJ, Kovar D. Selective laser flash sintering of 8-YSZ. J Am Ceram Soc. 2019;103(2):800–8.
25. Yang B, Cho J, Phuah XL, Wang H, Zhang X. Flash sintering of additively manufactured 3YSZ gears. J Am Ceram Soc. 2021;104(8):3828–32.
26. Gouws A, Hagen D, Chen A, Kardoulaki E, Beaman JJ, Kovar D. Onset of selective laser flash sintering of AlN. Int J Appl Ceram Technol. 2021;18(6):1988–98.
27. Gil-González E, Perejón A, Sánchez-Jiménez PE, Sayagués MJ, Raj R, Pérez-Maqueda LA. Phase-pure $BiFeO_3$ produced by reaction flash-sintering of Bi_2O_3 and Fe_2O_3. J Mater Chem A. 2018;6(13):5356–66.
28. Gil-González E, Perejón A, Sánchez-Jiménez PE, Román-González D, Pérez-Maqueda LA. Control of experimental conditions in reaction flash-sintering of complex stoichiometry ceramics. Ceram Int. 2020;46(18):29413–20.
29. Avila V, Yoon B, Ingraci Neto RR, Silva RS, Ghose S, Raj R, et al. Reactive flash sintering of the complex oxide $Li_{0.5}La_{0.5}TiO_3$ starting from an amorphous precursor powder. Scripta Mater. 2020;176:78–82.
30. Yoon B, Yadav D, Ghose S, Raj R. Reactive flash sintering: MgO and α-Al_2O_3 transform and sinter into single-phase polycrystals of $MgAl_2O_4$. J Am Ceram Soc. 2018;102(5):2294–303.
31. Jia Y, Su X, Wu Y, Bai G, Wang Z, Yan X, et al. Fabrication of lead zirconate titanate ceramics by reaction flash sintering of PbO-ZrO_2-TiO_2 mixed oxides. J Eur Ceram Soc. 2019;39(13):3915–9.
32. Xu C, Wang L, Bai B, Peng L, Cai S. Rapid synthesis of $Gd_2Zr_2O_7$ ceramics by flash sintering and its aqueous durability. J Eur Ceram Soc. 2020;40(4):1620–5.
33. Zhu Y, Ma B, Wang K, Sun Z, Ren K, Wang Y. Electric field-assisted solid-state reaction of $BaCO_3$-TiO_2 system. J Am Ceram Soc. 6572–8, 2021.
34. Avila V, Raj R. Reactive flash sintering of powders of four constituents into a single phase of a complex oxide in a few seconds below 700°C. J Am Ceram Soc. 2019;102(11):6443–8.
35. Liu J, Ren K, Ma C, Du H, Wang Y. Dielectric and energy storage properties of flash-sintered high-entropy $(Bi_{0.2}Na_{0.2}K_{0.2}Ba_{0.2}Ca_{0.2})TiO_3$ ceramic. Ceram Int. 2020;46(12):20576–81.
36. Liu D, Peng X, Liu J, Chen L, Yang Y, An L. Ultrafast synthesis of entropy-stabilized oxide at room temperature. J Eur Ceram Soc. 2020;40(6):2504–8.
37. Mao H-R, Guo R-F, Cao Y, Jin S-B, Qiu X-M, Shen P. Ultrafast densification of high-entropy oxide $(La_{0.2}Nd_{0.2}Sm_{0.2}Eu_{0.2}Gd_{0.2})_2Zr_2O_7$ by reactive flash sintering. J Eur Ceram Soc. 2021;41(4):2855–60.
38. Jesus LM, Silva RS, Raj R, M'Peko J-C. Electric field-assisted flash sintering of $CaCu_3Ti_4O_{12}$: Microstructure characteristics and dielectric properties. J Alloys Compd. 2016;682:753–8.
39. Jesus LM, Silva RS, M'Peko J-C. Ultrafast synthesis and sintering of materials in a single running experiment approach by using electric fields. J Adv Ceram. 2019;8(2):265–77.
40. Avila V, Yoon B, Ghose S, Raj R, Jesus LM. Phase evolution during reactive flash sintering of $Li_{6.25}Al_{0.25}La_3Zr_2O_{12}$ starting from a chemically prepared powder. J Eur Ceram Soc. 2021;41(8):4552–7.
41. Yoon B, Avila V, Raj R, Jesus LM. Reactive flash sintering of the entropy-stabilized oxide $Mg_{0.2}Ni_{0.2}Co_{0.2}Cu_{0.2}Zn_{0.2}O$. Scripta Mater. 2020;181:48–52.
42. Su X, Bai G, Zhang J, Zhou J, Jia Y. Preparation and flash sintering of $MgTiO_3$ nanopowders obtained by the polyacrylamide gel method. Appl Surf Sci. 2018;442:12–9.
43. Kumar A, Sharma G, Aftab A, Ahmad MI. Flash assisted synthesis and densification of five component high entropy oxide (Mg, Co, Cu, Ni, Zn)O at 350°C in 3 min. J Eur Ceram Soc. 2020;40(8):3358–62.

44. Ren K, Cao Y, Chen Y, Shao G, Dai J, Wang Y. Flash sintering of $Na_3Zr_2(SiO_4)_2(PO_4)$ solid-state electrolyte at furnace temperature of 700°C. Scripta Mater. 2020;187:384–9.
45. Monte RD, Kašpar J. Nanostructured CeO_2–ZrO_2 mixed oxides. J Mater Chem. 2005;15(6):633–48.
46. Furler P, Scheffe J, Gorbar M, Moes L, Vogt U, Steinfeld A. Solar thermochemical CO2 splitting utilizing a reticulated porous ceria redox system. Energy Fuels. 2012;26(11):7051–9.
47. Valdez JA, Byler DD, Kardoulaki E, Francis JSC, McClellan KJ. Flash sintering of stoichiometric and hyper-stoichiometric uranium. J Nucl Mater. 2018;505:85–93.
48. Ingraci Neto RR, McClellan KJ, Byler DD, Kardoulaki E. Controlled current-rate AC flash sintering of uranium dioxide. J Nucl Mater. 2021;547:152780.
49. Gates-Rector S, Blanton T. The powder diffraction file: a quality materials characterization database. Powder Diffraction. 2019;34(4):352–60.
50. Yashima M, Arashi H, Kakihana M, Yoshimura M. Raman scattering study of cubic-tetragonal phase transition in $Zr_{1-x}Ce_xO_2$ solid solution. J Am Ceram Soc. 1994;77(4):1067–71.
51. Ding Y, Long X, Peng S, Tan Z, Zhang D, Lu X. Phase evolution and chemical durability of $Zr_{1-x}Ce_xO_2$ ($0 \le x \le 1$) ceramics. Int J Appl Ceram Technol. 2018;15(3):783–91.
52. Varez A, Garcia-Gonzalez E, Sanz J. Cation miscibility in CeO_2–ZrO_2 oxides with fluorite structure. A combined TEM, SAED and XRD Rietveld analysis. J Mater Chem. 2006;16(43):4249–56.
53. Varez A, Garcia-Gonzalez E, Jolly J, Sanz J. Structural characterization of $Ce_{1-x}Zr_xO_2$ ($0 \le x \le 1$) samples prepared at 1650°C by solid state reaction. J Eur Ceram Soc. 2007;27(13-15):3677–82.
54. Achary SN, Sali SK, Kulkarni NK, Krishna PSR, Shinde AB, Tyagi AK. Intercalation/deintercalation of oxygen: a sequential evolution of phases in Ce_2O_3/CeO_2−ZrO_2 pyrochlores. Chem Mater. 2009;21(24):5848–59.
55. Lee TA, Stanek CR, McClellan KJ, Mitchell JN, Navrotsky A. Enthalpy of formation of the cubic fluorite phase in the ceria–zirconia system. J Mater Chem. 2011;23(4):1105–12.
56. Morikawa A, Yamamura K, Suda A, Tanabe T, Nobukawa T, Chiba A, et al. Phase transformation behavior of a pyrochlore-type CeO_2-ZrO_2 binary compound. J Am Ceram Soc. 2015;98(2):659–62.

SUPPORTING INFORMATION

Additional supporting information may be found in the online version of the article at the publisher's website.

How to cite this article: Ingraci Neto RR, Kardoulaki E, Valdez JA. The influence of the processing parameters on the reactive flash sintering of ZrO_2-CeO_2. J Am Ceram Soc. 2022;105:3937–3948.
https://doi.org/10.1111/jace.18426